

# The circumnuclear material in the Galactic Centre: A clue to the accretion process

R.H. Sanders

*Kapteyn Astronomical Institute, P.O. Box 800, 9700 AV Groningen, The Netherlands*

received: ; accepted:

## ABSTRACT

On the basis of “sticky particle” calculations, it is argued that the gas features observed within 10 pc of the Galactic Centre– the circumnuclear disk (CND) and the ionized gas filaments– as well as the newly formed stars in the inner one parsec can be understood in terms of tidal capture and disruption of gas clouds on low angular momentum orbits in a potential containing a point mass. The calculations demonstrate that a dissipative component forms a “dispersion ring”, an asymmetric elliptical torus precessing counter to the direction of rotation, and that this shape can be maintained for many orbital periods. For a range of plausible initial conditions, such a structure can explain the morphology and kinematics of the CND and of the most conspicuous ionized filament. While forming the dispersion ring, a small cloud with low specific angular momentum is drawn into a long filament which repeatedly collides with itself at high velocity. The compression in strong shocks is likely to lead to star formation even in the near tidal field of the point mass. This process may have general relevance to accretion onto massive black holes in normal and active galactic nuclei.

## 1 INTRODUCTION

Between two and five parsecs from the centre of the Galaxy, there is a ring of neutral and molecular gas which is usually referred to as the circumnuclear disk or CND (Genzel et al. 1994 and references therein). This feature is a clumpy, turbulent torus-like structure with a radial velocity field which is well-approximated by rotation about the dynamical centre of the Galaxy. Within the CND there is a central cavity where the overall gas density is significantly lower, but where filaments of ionized gas are detected both in free-free continuum radiation at radio wavelengths (Ekers et al. 1983, Lo & Claussen 1983) and in  $\text{Ne}^+$  line emission at infrared wavelengths (Serabyn & Lacy 1985). The ionized gas filaments, which may extend beyond the central cavity, have a very distinct morphology– sometimes called the “mini-spiral”. The total mass of the ionized gas is quite low– less than  $100 M_\odot$ . The radial velocity, as measured in the  $12.8 \mu\text{m}$   $\text{Ne}^+$  line (Serabyn et al. 1988) and in various hydrogen recombination lines (Schwarz et al. 1989, Roberts & Goss 1993, Herbst et al. 1993), indicate several distinct kinematic features having a systematic variation of radial velocity with position. The most conspicuous of these features is the Northern Arm and its extension to the west, designated the “extended Northern Arm” by Serabyn et al. (1988); it appears to wrap around the unresolved non-thermal radio continuum source, Sgr A\* which may be identified with a black hole having a mass possibly as large as  $3 \times 10^6 M_\odot$ .

Also within the inner one parsec there is a cluster of young stars with a projected density which increases to within a tenth of a parsec of Sgr A\* (Genzel et al. 1996). This cluster constitutes a trivial fraction of the mass of old bulge stars

within this volume ( $\approx 10^4 M_\odot$  or about 1% of the stellar mass, Morris & Serabyn 1996), but contributes most of the luminosity and all of the ionizing radiation in the central parsec. In particular, this cluster of stars is the source of ionization for the mini-spiral and the inner edge of the CND (Allen et al. 1990, Eckart et al. 1993, Krabbe et al. 1995).

There is now very strong dynamical evidence for a mass concentration in excess of  $2 \times 10^6 M_\odot$  centered at or near Sgr A\*. This is indicated by the high velocities seen in the ionized gas filaments near Sgr A\* and by the apparent increase in the measured radial velocities of the young stars with decreasing distance from Sgr A\*. The recent observation of proper motion of the bright young stars in the central few arcseconds (Eckart & Genzel 1996) make this conclusion almost inescapable; one cannot appeal to an anisotropic velocity distribution of these stars to account for an increase in only the line-of-sight velocity dispersion. But given the existence of such a mass concentration, it is difficult to understand the distribution and even the presence of the cluster of young stars (Allen & Sanders 1986, Sanders 1992). The estimated lifetime of the bright blue stars is on the order of a few million years. In the inner few tenths of a parsec this would correspond to more than 100 orbit times, so one would expect that the cluster should be thoroughly phase-mixed on this time scale. Yet the appearance is rather patchy and unmixed, with the centroid of the 20 or so most luminous stars comprising the IRS 16 complex lying distinctly to the southeast of Sgr A\* by about one second of arc (Eckart et al. 1993). Moreover, the formation of stars within a few tenths of a parsec of a massive black hole is quite problematic, because the density required for gravitational collapse

in the strong tidal field, the Roche limit, is

$$\rho > 1.5 \times 10^{-13} \frac{M_h}{10^6 M_\odot} \left( \frac{0.1 \text{ pc}}{r} \right)^3 \text{ g/cm}^3 \quad (1)$$

which is far greater than the observed or implied gas densities in the central cavity.

It has been suggested that the ionized gas streamers may in fact be small gas clouds on low angular momentum orbits which pass within 0.2 pc of the central black hole (Ekers et al. 1983, Lo & Claussen 1983, Serabyn et al. 1988). The idea is that such a cloud would be tidally stretched along its orbit, and this has led to modeling the morphology and kinematics of each of the various individual features (see Fig. 2) by motion along Keplerian orbits appropriately projected onto the plane of the sky (Serabyn et al. 1988, Herbst et al. 1993, Roberts et al. 1996). It has been further suggested that the young stars seen in this region may have resulted from previous infall episodes; the gas densities behind the strong shocks expected in gas streams colliding with high velocity ( $> 200 \text{ km/s}$ ) could approach the Roche limit (Phinney 1988).

For understandable reasons, these original models for the gas filaments have been quite simple; the objective has been to provide a first order description of the observed shape and motion of the features and to obtain limits on a central mass. Nonetheless, with such simple models, the kinematics and morphology of features such as the extended Northern Arm have been quite accurately reproduced (Herbst et al. 1993, Roberts et al. 1996). On the basis of this work it is difficult to avoid the conclusion that the motion of the ionized gas filaments is primarily orbital and that there is a large central mass concentration.

Given the likely existence of a massive black hole at the Galactic Centre, the structure and kinematics of the surrounding material— the CND, the ionized filaments, and the cluster of young stars— offers a unique close-up view of the accretion process which may be relevant to galactic nuclei in general. Here, using a sticky particle code, I consider this accretion process in the context of tidal disruption of clouds on low angular momentum orbits about the dynamical centre. The gravitational potential in which the gas clouds move is that of a point mass and an extended spherically symmetric mass distribution similar to that of an isothermal sphere as suggested by near-infrared observations of the stellar component in the central region (Genzel et al. 1996). Because of viscous dissipation the tidal debris from such a cloud forms an elliptical annulus of gas which precesses about the centre opposite to the sense of particle motion.

Such a structure can be described as a “dispersion ring”, to borrow an old term from galactic dynamics (Lindblad 1956, Oort 1965). This is an ensemble of non-circular orbits in an arbitrary axisymmetric gravitational potential. Each of these orbits is a closed ellipse in some rotating frame; in certain circumstances it is possible to organize these orbits over some range in energy or radius so that they precess with about the same angular velocity. Then a non-axisymmetric structure, in this case an off-set elliptical annulus, can be constructed in an axisymmetric potential— a structure which may persist for a number of characteristic rotation periods (see Figs. 10a and 10c), as is the case for elliptical accretion discs in a point-mass potential (Syer & Clarke 1992). Here

the self-organization of the gas into such a dispersion ring develops through the process of dissipation.

For a roughly spherical cloud with a radius of about 2 pc, initially located between 6 and 10 pc of the centre on an orbit which carries it within 3 or 4 parsecs of the centre, the resulting dispersion ring is broad and asymmetric with a central cavity of 1 to 2 pc— similar in structure and kinematics to the CND. This similarity supports the idea that the CND has resulted from the disruption of a cloud about one million years ago.

At least some of the ionized gas filaments in the central cavity may have a similar explanation, although in this case, a small cloud with a radius less than 0.5 pc at an initial distance of 2 and 3 pc from the centre must pass within about 0.2 pc of the central point mass. Then the resulting highly elliptical dispersion ring has a structure and kinematics very similar to that observed in the extended Northern Arm, and it persists for much longer than an orbital period ( $\approx 5 \times 10^4$  years). On the first passage by the point mass, tides stretch the cloud into a long filament. On subsequent passages, while forming the dispersion ring, the filament intersects itself at high velocity, and this can lead to compression in strong shocks and probable star formation. Thus many of the young stars seen in this region may have resulted from this or earlier such accretion episodes; in any case, the gas now comprising the extended Northern Arm may well be only a bare remnant of the original cloud.

All of this suggests that, in general, accretion onto massive black holes in the nuclei of spiral galaxies may proceed by such tidal capture of low angular momentum clouds. If so, the accretion process is likely to be highly episodic but also highly inefficient with most gas disappearing in star formation rather than being consumed by the black hole. The essential ingredient is a clumpy, turbulent interstellar medium in the inner few hundred parsecs. Such a medium is directly observed in the Galaxy and may be an attribute of the central regions of many spiral galaxies.

In all that follows the distance to the Galactic Centre is taken to be 8.5 kpc.

## 2 CALCULATIONS

Earlier calculations of tidally stretched cloud models which take into account gas dynamical effects include those of Quinn & Sussman (1985) and Bottema & Sanders (1986). Quinn & Sussman follow the motion of particles under the influence of gravity and a drag force induced by an ambient medium. In order to significantly affect the motion of the material the ambient medium must have a density approaching that of the filaments. Bottema & Sanders carry out a fully hydrodynamic simulation which suggests that a rather complex structure, not dissimilar to that observed in the Galactic Centre, can form due to multiple passes of material from a single cloud. However, the technique applied here, an Eulerian first order scheme with a square grid and transparent boundaries, is inappropriate to this problem (e.g., material leaving the grid can never return). The ideal method is a sticky particle or SPH routine because motion of material can be followed arbitrarily close to, or far from, the central point mass. Moreover, the fact that orbital motion is highly supersonic implies that the most

important gas dynamical effect will be dissipation is strong shocks rather than ordinary pressure gradient forces; it is unnecessary to apply full SPH to model the essential effects (see Whitehurst 1988 for a discussion of this issue).

In the present calculation the gravitational potential is that of point mass embedded in an extended mass distribution (the old stellar population) which makes a significant contribution to the force at radial distances larger than about 1 pc. The density distribution of the dominant stellar component is taken to be spherically symmetric and given by

$$\rho_* = \rho_o \left(1 + \frac{r}{r_c}\right)^{-2}. \quad (2)$$

where the central density is  $\rho_o = 2.67 \times 10^7 M_\odot \text{pc}^{-3}$  and the core radius is  $r_c = 0.085$  pc. When combined with a  $2.5 \times 10^6 M_\odot$  point mass at  $r = 0$ , this yields an mass distribution within the inner 5 pc which is identical, within the observational errors, to that derived by Genzel et al. (1996) on the basis of the Jeans equation using the measured projected stellar density distribution and velocity dispersion. The total gravitational force in the inner few parsecs is then given by

$$f = \frac{8.9 \times 10^2}{r^2} \left[ \frac{r}{r_c} - \arctan\left(\frac{r}{r_c}\right) \right] + \frac{4.3 \times 10^3}{r^2} \left( \frac{M_{bh}}{10^6 M_\odot} \right) (\text{km/s})^2 \text{pc}^{-1}. \quad (3)$$

where  $M_{bh}$  is the mass of the central object. In all calculations described below,  $M_{bh} = 2.5 \times 10^6 M_\odot$  which is the value indicated by the stellar kinematics (Genzel et al. 1996),

The calculations follow the motion of 4000 particles in the orbital plane; i.e., the calculation is two dimensional. This can be justified by full three-dimensional calculations (E. Hartlief, private communication 1996) which demonstrate that when dissipation is included a spherical cloud of particles collapses very rapidly into the orbital plane on the first passage by the point mass (half the particles with positive velocity perpendicular to the plane collide with the half traveling in the opposite direction). The equations of motion for the particles are integrated by means of a fourth-order Runge-Kutte technique with the time step continually adjusted to achieve a specified level of accuracy.

The technique for including dissipation is similar to earlier methods (e.g. Schwarz 1981, Whitehurst 1988, Jenkins & Binney 1994) and combines aspects of sticky particle and SPH algorithms. In two dimensions every particle is a circle with a radius  $\sigma$  chosen to be sufficiently large such that each particle overlaps about 10 of its neighbours. At any time step every particle adjusts its velocity slightly to reduce the radial velocity difference with each neighbour provided that the radial velocity difference is negative (i.e., the particles are approaching). For two particles  $i$  and  $j$ , we take  $\mathbf{V}_{ij}$  to be the component of relative velocity along the line joining the two particles ( $\mathbf{V}_{ij}$  is a vector at the position of particle  $i$  pointing away from particle  $j$ ). If  $r_{ij}$  is the separation between particle  $i$  and  $j$  then in time step  $\Delta t_k$  particle  $i$  changes its velocity by an amount given by the vector sum

$$\Delta \mathbf{v}_{ik} = \alpha_k \sum_j^{r_{ij} < \sigma} \mathbf{V}_{ij} \quad (4)$$

where

$$\alpha_k = \Delta t_k / \Delta t_s \quad (5)$$

The strength of the interaction is proportional to  $\alpha_k$ . Here  $\Delta t_s$  is a standard time interval (a dissipation time scale) which is typically taken to be 0.04 of a characteristic orbit time in the inner few parsecs ( $\Delta t_s \approx 4000$  years).

This is an algorithm for including a bulk viscosity in which every particle's velocity is adjusted proportionally to the local velocity divergence, but only if that divergence is negative (i.e., the flow is converging). The interaction strength,  $\alpha_k$  depends upon the duration of the time step. If this were not the case, then, when considerations of numerical accuracy force the time step to be very short (as when several particles are near the point mass), the entire fluid would become unrealistically more viscous.

In the calculations shown the motion of two interacting particles is not effected by the transverse component of their relative velocity; that is to say, shear viscosity is explicitly excluded. This is done because the primary mechanism determining the evolution of the debris is dissipation, and this is adequately modeled by bulk viscosity. Shear viscosity, when included, has no significant effect on the results, but it does tend to make a fluid which is already quite possibly too sticky even more so.

It is evident that inelastic interaction described by eq. 4 conserves the linear momentum of two interacting particles. The total angular momentum of the ensemble of particles is also conserved; although, the angular momentum may be redistributed among particles while the total energy decreases. Gridding is used to speed up the search for neighbours, but, because of the circular neighborhood, the interaction is isotropic and bears no imprint of the imposed Cartesian grid. As is typical in such calculations, there is some tendency for the particles to bunch together; this tendency is greater for smaller values of  $\Delta t_s$ . Nonetheless, the gross features of the calculation turn out to be rather insensitive to the exact values of  $\sigma$  and  $\Delta t_s$  provided that each particle actually overlaps several other particles at any given time.

### 3 SIMULATION OF THE CND

The CND as observed in HCN, together with the ionized gas filaments as seen in the 6 cm continuum, is shown in Fig. 1 which is reproduced from the paper of Güsten et al. (1987). In a recent review, Morris & Serabyn (1996) emphasize the asymmetry of the CND and its probable transient nature. From inspection of Fig. 1 it is evident that Sgr A\*, presumed to be at the dynamical centre of the Galaxy, is not at the centre of the central cavity of the CND but is closer to its western edge. Moreover, the molecular gas is significantly more tenuous on the eastern side of the center. The ionized gas associated with the inner edge of the CND is also asymmetrically distributed; the free-free emission does not form a complete ring but only appears as the Western Arc of the mini-spiral. The outer part of the CND is clearly asymmetric and more extended to the south than to the north. All of this suggests that the CND may be formed by capture and disruption of a passing cloud, and this is the possibility pursued here.

The simulation is that of a clumpy cloud on a low angular momentum orbit in the gravitational field described above (eq. 3). The initial radius of the cloud is approximately 2 pc and it is located at 6.5 pc from the Galactic Centre. The cloud consists of 40 sub-units (clumps) each comprised of 100 particles, and the velocity dispersion between the clumps is 40 km/s. The clumps have a systematic velocity only in the tangential direction which may be expressed in terms of the circular velocity  $V_c$ — the velocity required for a circular orbit at this radius—

$$V_t = fV_c. \quad (6)$$

Here  $f=0.4$  or  $V_t \approx 40$  km/s. Therefore, the cloud will fall toward the dynamical centre. Such an initial configuration might result from the collision of two oppositely moving clouds, not an unlikely event in a highly inhomogeneous and turbulent medium. Given that the mass of the CND is roughly  $10^4 M_\odot$  (Mezger et al. 1996), the mean particle density of the initial cloud is approximately  $10^4 \text{ cm}^{-3}$ ; the cloud would be stable against gravitational collapse if the velocity dispersion exceeds 5 km/s.

The 4000 sticky particles are characterized by a radius  $\sigma = 0.1$  pc, and an interaction time interval of  $\Delta t_s = 4000$  years (eqs. 4 & 5). This means that velocity of two interacting particles can change by as much as their velocity of approach over 4000 years. The duration of the time step typically varies between 50 and 250 years, so the actual change over a time step in the velocity of two interacting particles is only a few percent of the approach velocity.

The results are shown in Fig. 2 which is a time sequence showing the passage of this cloud in the orbital plane. Each frame is a snapshot of the morphology of the cloud at the indicated time, in units of a million years, since the beginning of the infall. The cloud, on its first passage by the point mass, is stretched by the tidal force into a long filament. Subsequently, the filament wraps about the centre and collides with itself once per orbital period in the first two or three periods (note that the orbit time at 3.5 pc from the centre is about  $2 \times 10^5$  years). After two or three characteristic orbit times ( $\approx 5 \times 10^5$  years), the cloud has settled into an asymmetric circumnuclear ring with a central cavity. If the force were strictly that of a point mass the tidal debris would form a Keplerian ellipse, fixed in the orbital plane, which would persist for many orbital periods. Indeed, in such a calculation with a  $1/r^2$  force law, the distribution of particle orbits show no tendency for circularization over 10 characteristic orbital periods which is consistent with the results of Syer & Clarke (1992) on Keplerian elliptical accretion discs. However, in the case considered here, because of the contribution of the Galactic potential the force is not  $1/r^2$ . This means that different parts of the elliptical accretion disc precess at different rates, and the process of circularization is more rapid than in the Keplerian case. But during this process, the tidal debris temporarily forms a broad elliptical ring with a one-arm spiral which is precessing counter to the sense of particle motion— a “dispersion ring” as defined in the Introduction. The ring is fully developed after a million years, and gradually, over two or three million years, the central cavity fills in and the ring contracts while becoming more circular.

The tidal debris, as it appears in the seventh frame of Fig. 2 ( $t=0.85$ ), provides a fair description of the CND.

Rotating this structure clockwise by 130 degrees, tilting the positive y-axis forward about the x axis by 60 degrees (the inclination of the orbital plane) and rotating the negative x axis (the line-of-nodes) to a position angle of 35 degrees with respect to the vertical (north), the ring would appear as shown in Fig. 3a which is on the same scale as Fig. 1. These are typical projection parameters for the CND where the northwestern side is assumed to be the near side. The arrows indicate the magnitude and direction of the velocity projected onto the plane of the sky and the “X” marks the position of Sgr A\*; the straight line is the line-of-nodes. A contour map of the gas surface density is shown in Fig. 3b. It is evident that the size and the asymmetry of the CND are approximately reproduced. The two dimensional radial velocity field is shown in the form of a contour map in Fig. 3c, and the radial velocity at the inner edge of the ring as a function of position angle is compared to the observations of Güsten et al. (1987) in Fig. 4.

In both morphology and kinematics the agreement between the observations and model is reasonable. In the model, the densest part of the ring with the sharpest inner boundary is the western side, nearest to the point mass; the eastern side of the ring is rather tenuous and ill-defined. This is due to the fact that the elliptical orbits in the dispersion ring crowd together at the peri-centre. Looking back at Fig. 1 we see that the distribution of molecular gas has just this asymmetry. This is not just an aspect of the particular simulation; in the dispersion ring model of the CND, that part of the inner boundary which is closest to the dynamical centre, will always have the highest gas density due to the orbit crowding. Moreover, because of the higher gas density along the western rim of the cavity, it is likely that the emission measure of the ionized gas is greater here than elsewhere along the inner boundary; that would be consistent with the fact that only this part of the cavity boundary reveals itself as an ionized filament (the Western Arc).

The model considered here, with the adopted orientation, reproduces the observed outer asymmetry of the CND, the extension to the south, because of the one-arm spiral feature. In the projection required for the inner edge asymmetry, this feature does extend to the south provided that the near side of the CND is the northwestern side. However, an aspect of the observed morphology which is not reproduced by this simple model is the extension to the northwest. This feature might result from initial irregularities in the shape of the cloud or from a separate infall event (e.g., associated with the Northern Arm).

It seems significant that the same model and orientation parameters which reproduce the overall morphological aspects of the CND also give the closest match to the observed kinematics. In particular, the ridge of positive velocity material to the west of Sgr A\* (Fig. 3c) is a conspicuous aspect of the observations (Güsten et al. 1987) but would not be a property of an axisymmetric disc. The asymmetry in the observed kinematics of the inner edge (Fig. 4) has been attributed to the warping of the plane of the CND. However, the model here reproduces these asymmetries via gas motion on offset elliptical streamlines.

All of these distinct aspects of morphology and kinematics— the outer extension to the south, the highest density edge on the western side, the kinematic asymmetry of the inner boundary, the appearance of the positive

velocity ridge to the west— can, for the observed sense of rotation, only be reproduced for a specific orientation of the model CND in space; that is to say, the near side is the northwestern side in the context of this scenario. This is because the asymmetric gas distribution and kinematics break the usual nearside-farside degeneracy of axisymmetric structures. This is a prediction which is independent of the details of the orbital initial conditions; the consequence is that the proper motion vectors of the gas must be in the sense shown in Fig. 3a.

Any calculation in which a cloud with a size of two or three parsecs having an initial galacto-centric distance of six to eight parsecs and a tangential velocity about half that required for a circular orbit will lead to roughly the same structure. The essential— and model-free— results are that the tidal debris will form an elliptical and asymmetric dispersion ring which persists for at least a million years and that the central cavity is also asymmetric with the side nearer the point mass having a sharper inner boundary and higher gas density. This structure, with a very specific orientation in space, provides a plausible representation of the CND.

#### 4 THE IONIZED FILAMENTS

The ionized filaments in the central cavity of the CND are shown in greater detail in Fig. 5. The most conspicuous and coherent of these features is the extended Northern Arm which has a radial velocity that varies systematically with position over 30 seconds of arc as it sweeps around Sgr A\*. Due to the large gradient in radial velocity near Sgr A\*, it is certain that this feature actually does pass within about 0.2 pc of Sgr A\*— a true distance which is comparable to the projected distance (Herbst et al. 1993, Roberts et al. 1996). The structure of the Northern Arm is clearly delineated in the 12.4  $\mu$ m continuum radiation from hot dust seen in Fig. 6 (Gezari, Dwek & Varosi 1996). The “Eastern Arm” appears less conspicuous in this mid-infrared emission, and it is now quite clear that the “Western Arc” is the ionized inner edge of the circumnuclear ring (Lo & Claussen 1983, Roberts & Goss 1993). Features such as the extended Northern Arm may result from the same process as that giving rise to the CND. If so, then because this filament passes so near Sgr A\*, the specific angular momentum of the original cloud ( $f$  in eq. 6) must be smaller than that required for formation of the CND.

Fig. 7 is again a time sequence of the evolution of tidal debris resulting from an passage of a small cloud (a “cloudlet”) on a very low angular momentum orbit. Initially the cloudlet is round with a radius of 0.4 pc, and the centre of the cloudlet is at a distance of 2.4 pc from the Galactic Centre, moving tangentially (counterclockwise) with  $f=0.2$  in eq. 6 (about 20 km/s). In this case the cloudlet has zero internal velocity dispersion. The interaction properties of the sticky particles are  $\sigma = 0.02$  pc and  $\Delta t_s = 4000$  years. The linear scale of the frames in Fig. 7 is a factor of three smaller than those of Fig. 2 and the indicated times, again in units of  $10^6$  years, are a factor of 10 shorter than in the case of the CND simulation due to the close approach of the cloud particles to the point mass. Such a cloudlet could be a particularly low angular momentum clump in the larger

cloud forming the CND or it could result from a subsequent accretion event. The difference in time scales would seem to argue in favor of the latter, but more will be said about this below. If the mass of this original cloudlet were comparable to that of the ionized gas in the filaments ( $\approx 100 M_\odot$ ), then the original density would be on the order of  $10^4 \text{ cm}^{-3}$  as in the cloud forming the CND. Overall this cloudlet would have the properties of an observed clump in the CND (Genzel et al. 1994). Such clumps are subject to tidal disruption at distances between two to three parsecs from the center (eq. 1). It may be that the clumps maintain their integrity by turbulent pressure (collisions) and that occasionally such a collision will lead to the sort of low angular momentum cloudlet required here (the clumps may also be denser as suggested by the analysis of Jackson et al. 1993).

As in the previous simulation the cloud is tidally stretched into a long filament which repeatedly plunges toward the point mass, colliding with itself as in the fourth frame ( $t=0.075$ ). By  $2 \times 10^5$  years a fairly coherent and relatively long-lived elliptical dispersion ring is formed which precesses counter to the direction of rotation with a angular velocity of  $\Omega \approx 26 \text{ km/s pc}^{-1}$  (i.e., the precession period is about  $2.5 \times 10^5$  years). The time for this structure to settle into a more axisymmetric accretion disk depends upon the viscous dissipation but may be as long as  $10^6$  years. This circularization time-scale, in terms of orbital periods, is longer than that of the CND cloud because of the smaller initial size of the cloud; there is less differential precession over the narrow dispersion ring.

On the way to forming the dispersion ring, streams of gas collide repeatedly with high velocity, as at  $t = 0.10$ . The structure at these epochs is not unlike that seen in the ionized gas streamers, and it is tempting to identify this morphology with that of the three arm spiral. Indeed with the appropriate projection the narrow filament can be matched with the Northern Arm, Eastern Arm and Bar. However, such a projection fails to reproduce the observed dependence of radial velocity on position, particularly in the well-studied extended Northern Arm. Both morphologically and kinematically, this feature appears to be distinct from the Eastern Arm (see Fig. 6), and the two should probably not be modeled as part of the same structure (Roberts & Goss 1993).

The morphology and the kinematics of the extended Northern Arm are well-modeled by dispersion ring as it appears, for example, in the eighth frame ( $t = 0.175$ ). Rotating the frame clockwise by 80 degrees in the orbital plane, tilting the positive y-axis forward by 50 degrees (the inclination) and rotating the negative x-axis (the line-of-nodes) to a position angle of 35 degrees with respect to north, the structure appears as in Fig. 8a where again arrows indicate the sense and magnitude of proper motion. This projected dispersion ring, at its northern most extent, appears rather thick in comparison with the observed ionized filament. This is consistent with the Northern Arm being the inner ionized edge of a broader contiguous region of neutral and molecular gas, the so-called “Northern Intruder” (Davidson et al. 1992, Jackson et al. 1993).

A contour map of the projected density is shown in Fig. 8b. Here it is evident that the eastern section of the ring is more dense and, if ionized, would have a significantly higher emission measure than the more tenuous western side. This

is consistent with the fact that the extended Northern Arm appears as an incomplete elliptical ring; i.e., no western component is clearly observed. Comparing Fig. 8b with Fig. 6 (the scale is the same) we see that the morphology of the Northern Arm is generally consistent with dispersion ring model. The points in Fig. 8b indicate the positions where the radial velocity has been measured in Br $\gamma$  line emission by Herbst et al. (1993); again the coincidence with the projected dispersion ring is reasonable.

The radial velocity field is shown as a contour map in Fig. 8c. This agrees with the run of radial velocity observed in the Ne<sup>+</sup> line (Serabyn et al. 1988) as well as in infrared and radio hydrogen recombination lines (Herbst et al. 1993, Roberts et al. 1996). Another representation of the velocity field of this structure is shown in Fig. 9 which is the radial velocity at the inner edge as a function of position angle (as in Fig. 4 for the CND). Also shown are the observations of the extended Northern Arm radial velocity given by Herbst et al. (1993). The evident agreement lends credibility to this scenario.

It is perhaps more than fortuitous that the projection of this dispersion ring giving the closest agreement with both kinematics and morphology of the extended Northern Arm implies the orbital plane of this feature almost coincides with that of the CND; the angle between the two planes is 10 degrees. Here, in both cases, it is assumed that the northwestern edge is the near side (observationally, this issue remains unclear, see Mezger et al. 1996). An alternative model is possible with southwestern side as the near side (the proper motion vectors would be oppositely directed to those shown in Fig. 8a), but then the plane of the Northern Arm would not coincide with that of the CND (the specific orientation of the CND is favored in this picture by the model fit to the morphological and radial velocity asymmetries). The probable near coincidence of the two planes would suggest that there is a rather close relationship between the extended Northern Arm and the CND— that both originated from low angular momentum material in the same plane and possibly from the same accretion event.

It is also noteworthy that this structure can only be reproduced if a point mass is present; if the central object has a mass less than  $10^6 M_{\odot}$  then the tidal stretching into a long filament does not occur. Although this adds very little to earlier arguments on the necessity of a massive object at the Galactic Centre, it is also of interest that the deviation from  $1/r^2$  attraction in the central two parsecs due to the contribution of the extended stellar system leads to strong shocks during the formation of the precessing dispersion ring. Such shocks are necessary to obtain the compression required for star formation in the near vicinity of the black hole (as discussed in the next section). This consideration limits the mass of the central object to be less than about  $3 \times 10^6 M_{\odot}$ ; otherwise the potential is too near Keplerian and there are no strong shocks.

The only conspicuous structure which is not accounted for in this picture is the Eastern Arm. In fact, this structure cannot be in the orbital plane of the extended Northern Arm if its motion is also orbital. Perhaps this feature traces a separate infall event or is part of the ionized ragged inner boundary of the CND (Serabyn 1988, Morris & Serabyn 1996).

## 5 STAR FORMATION IN STRONG SHOCKS

Gas transported inward toward the black hole on highly elongated and intersecting orbits, as in Fig. 7 (at  $t=0.1$  for example) will form extremely strong shocks at the point of intersection. The post-shock density in streams colliding with relative velocities in excess of 100 km/s could exceed the Roche limit (eq. 1) for star formation at a tenth of a parsec from the hole (Phinney 1988). This then provides a natural mechanism for formation of the young stars seen in the central parsec of the Galaxy.

The triggering of star formation in regions of strong gas compression is easily modeled in the simulation described here because the divergence of the velocity field can be estimated. At time  $k$  and at the location of the  $i^{th}$  particle this is

$$-(\nabla \cdot v)_{ik} = \frac{|\Delta \mathbf{v}_{ik}|}{\alpha_k \sigma} \quad (7)$$

where  $\Delta \mathbf{v}_{ik}$  is given by eq. 4. Unsurprisingly, the region of largest gas compression is very near the black hole where streams intersect. We may assume that a gas particle at a given location becomes a star if the negative velocity divergence (compression) at that location exceeds some arbitrary threshold. Once a particle has been converted into a star the dissipation is turned off, and thereafter its motion is determined only by the force of gravity.

The cloud infall illustrated in Fig. 7 has been repeated using this algorithm for star formation with the compression threshold for star formation set at 2000 km/s/pc. Most of the star formation occurs during the first few passages of the cloud when the long filament intersects itself at a large angle. Snapshots of the gas and star distributions at a time of  $3.0 \times 10^5$  years (corresponding to more than one precession period for the dispersion ring) are shown in Figs. 10a and 10b respectively. By this epoch the gas has settled into the stable dispersion ring and the star formation has almost ceased. Roughly half of the original 4000 gas particles have been converted into stars. The star and gas distribution at  $5.5 \times 10^5$  years, almost one precession period later, are shown in Figs. 10c and 10d. The gaseous dispersion ring, as seen in Fig. 10c, is clearly present after two complete precession periods; it is a long lived and stable feature which can persist for more than a million years. The morphology and kinematics of this feature continue to resemble that of the extended Northern Arm for 10 to 20 orbit times.

Fig. 10 illustrates the effect of gas dissipation on the resulting morphology. The fact that strong dissipational forces arise when high velocity gas streams intersect gives rise to the coherent structure of the dispersion ring in which dissipation is minimized; in the language of modern dynamics, the dispersion ring appears as an “attractor” in the phase space of the system. The ensemble of stars, with no such mechanism for self-organization, slowly disperses throughout the available phase space. But, significantly, the time scale for phase mixing of the stellar orbits is rather long. This is because the stars are formed from the gaseous dispersion ring— i.e., in the 4-dimensional phase space the domain of initial conditions with which these particles are created is quite restricted. The rosette pattern of the stellar orbits is still evident as an underlying skeletal structure (Fig. 10b) after one complete precession period of the dispersion ring

or about 5 orbit times at one parsec. It takes 2 or 3 precession periods for the stellar orbits to become well mixed (Fig. 10d).

This scenario, therefore, can provide an explanation not only for the existence of young stars near a massive black hole but also for a spatial distribution of these stars which is not yet completely relaxed. Although stars can be formed a few tenths of a parsec from the black hole, the relevant time scale is not that of an orbital period in this small region, as previously supposed (Allen & Sanders 1986, Sanders 1992), but the precession period of the more extensive gaseous dispersion ring from which these stars have been formed. As is evident from Fig. 10d the phase mixing time scale for the stellar orbits is in excess of two precession periods of the dispersion ring— in this case more than half a million years— which is 100 times longer than the orbital period in the inner few tenths of a parsec. As the gas dispersion ring precesses it decays into a more axisymmetric torus on a time scale exceeding a million years.

Some of the young stars currently observed in the inner few tenths of a parsec may well have been formed quite recently out of the tidal debris traced by the observed filaments. However, given that the likely lifetime of the youngest stars is in excess of one-million years, many of these stars may have also been formed in recent infall events. Gas clouds with low angular momentum do not necessarily share the sense of Galactic rotation. Therefore, the fact that the youngest stars appear to possess a component of systematic counter-rotation (Genzel et al. 1996), may just reflect the direction of the original angular momentum vector of the tidally disrupted cloud from which these stars have formed.

## 6 CONCLUSIONS

It is now difficult to dispute the probable presence at the Galactic Centre of a black hole with a mass in excess of  $10^6 M_\odot$ . However, as has been pointed out many times before, the absence of the sort of activity normally associated with active galactic nuclei would imply that the Galactic Centre black hole is currently in a quiescent phase— that activity associated with massive black holes in galactic nuclei is episodic, and, by implication, that accretion in galactic nuclei is also episodic.

A schematic scenario of episodic accretion is that of a nucleus containing a black hole and a few dozen massive clouds with random rather than systematic motion (Sanders 1981). Occasionally a cloud directly encounters the black hole leading to Bondi accretion and the buildup of a short-lived accretion disk. This picture was somewhat refined by Bottetma and Sanders (1986) who showed that in such an encounter, the amount of material captured and the time scale for subsequent accretion could fuel a short ( $10^5$  year) outburst of Seyfert activity followed by 10 million years of inactivity.

The observations of the circumnuclear material in the Galactic Centre lend some support to this picture, although accretion events are not so simple as a direct encounter of a molecular cloud with a black hole. It appears that accretion actually proceeds through the tidal disruption and capture of clouds on low angular momentum orbits. This can lead to the formation of structures resembling the CND and the

ionized extended Northern Arm in the central cavity of the CND. The general pattern of such capture in the presence of a point mass is the tidal stretching of a cloud into a long filament which collides with itself before being organized into a long-lived, elliptical precessing dispersion ring. If the specific angular momentum of the captured cloud is low enough the gas streams intersect with high velocity which almost certainly leads to very active star formation even in the near tidal field of the black hole. Thus the accretion process is highly inefficient in the sense that much of the captured material forms stars rather than being accreted by the black hole.

All of this requires a very clumpy and turbulent interstellar medium in the inner few hundred parsecs of the Galaxy. But this is not an assumption because molecular line observations clearly reveal the presence of such a medium (see Morris & Serabyn 1996 and Mezger et al. 1996). Of course one might reasonably ask what provides a continuous supply of low angular momentum clouds and what supports the highly supersonic turbulence. Dynamical friction is one mechanism which can move massive molecular clouds from 200 pc inward to the centre on time scales less than  $10^9$  years (Stark et al. 1991). High turbulent velocities may be maintained by the continuing star formation and by the occasional flare-up of the black hole. It is likely that the low specific angular momentum of the clouds forming the CND and ionized filaments results from cloud-cloud collisions in the inner 5 to 10 pc.

In summary, the dispersion ring model has many of the observed properties of the CND— for example, an asymmetric central cavity with the gas density being much higher on the side nearest to the point mass at the dynamical centre. In addition, at least some of the ionized gas filaments in the central parsec (the extended Northern Arm) may also be identified with a highly elliptical dispersion ring. For a cloud with such low specific angular momentum, on the way to becoming a dispersion ring self-intersection of gas streams with high velocity will probably lead to star formation, and this could well be the origin of the very young massive stars actually observed in the central parsec of the Galaxy. Because the stars form from gas on a dispersion ring extending from 0.1 to 1 pc and occupying a restricted domain of the available phase space, phase mixing occurs on a time scale which is much longer than the characteristic orbit time in the inner few tenths of a parsec ( $10^6$  years instead of  $10^4$  years). Thus both the formation and unrelaxed distribution of stars in the near tidal field of the black hole may be understood in terms of this mechanism.

Many of these ideas are not new: i.e., the transient nature of the CND, the identification of the ionized filaments with tidally stretched clouds, star formation in strong shocks in colliding gas streams. The new aspect suggested by the sticky particle code applied in this work is the identification of the gaseous circumnuclear material with asymmetric elliptical dispersion rings formed by the tidal debris from clouds on low angular momentum orbits. The objective here is not to model precisely the morphology and kinematics of the CND and the ionized filaments; the parameter space of initial conditions is too large for that exercise to be particularly meaningful. Nonetheless, such models for the gas features seen in the inner few parsecs do make some predictions. For example, consistency with the morphological and

kinematic asymmetries of the CND (the dense inner boundary to the west, the outer extension to the south, the ridge of positive velocity to the west of Sgr A\*) gives preference to a specific spatial orientation: the northwestern side is the near side. Then, because the best fit dispersion ring model of the extended Northern Arm suggests that the plane of this feature coincides with that of the CND, the proper motion of individual gas clumps near Sgr A\*, if this could be measured, would have the directions shown in Fig. 8a; i.e., motion along the Northern Arm is toward Sgr A\*. Moreover, we might expect that the extended Northern Arm is a more complete elliptical structure (Fig. 9) with a faint western counterpart. Higher sensitivity recombination line observations might unveil the complete dispersion ring. For now, the overall similarity between the model and the observed morphology and kinematics of the CND and extended Northern Arm supports the plausibility of this scenario.

I am grateful to E. Hartlief for initial three-dimensional calculations of tidal disruption which demonstrate the validity of the two dimensional calculation applied here.

## REFERENCES

- Allen, D.A., Hyland, A.R., Hillier, D.J. 1990, MNRAS, 244, 706  
 Allen, D.A., Sanders, R.H. 1986, Nature, 319, 191  
 Bottema, R., Sanders, R.H. 1986, A&A, 158, 297  
 Eckart, A., Genzel, R., Hormann, R., Sams, B.J., Tacconi-Garman 1993, ApJ, L77  
 Eckart, A., Genzel, R. 1996, Nature, 383, 415  
 Ekers, R.D., van Gorkom, J.H., Schwarz, U.J., Goss, W.M. 1983, A&A, 122, 143  
 Genzel, R., Hollenbach, D., Townes, C.H. 1994, Rep.Prog.Phys., 57, 417  
 Genzel, R., Thatte, N., Krabbe, A., Kroker, H., Tacconi-Garman, L.E. 1996, ApJ, 472, 153  
 Güsten, R., Genzel, R., Wright, M.C.H., Jaffe, D.T., Stutzki, J., Harris, A.I. 1987, ApJ, 318, 124  
 Gezari, D., Dwek, E., Varosi, F. 1996, in IAU Symp.169, Unsolved Problems of the Milky Way (eds. L. Blitz & P. Teuben), Dordrecht: Kluwer, 231  
 Herbst, T.M., Beckwith, S.V.W., Forrest, W.J., Pipher, J.L. 1993, AJ, 105, 956  
 Jackson, J.M., Geis, N., Genzel, R., Harris, A.I., Madden, S., Poglitsch, A., Stacey, G.J., Townes, C.H. 1993, ApJ, 402, 173  
 Jenkins, A., Binney, J. 1994, MNRAS, 270, 703  
 Krabbe, A., Genzel, R., Eckart, A., Najarro, F., Lutz, D., Cameron, M., Kroker, H., Tacconi-Garman, L.E., Thatte, N., Weitzel, L., Drapatz, S., Geballe, T., Sternberg, A., Kudritzki, R. 1995, ApJ, 447, L95  
 Lacy, J.H., Achtermann, J.M., Serabyn, E. 1991, ApJ, 380, L71  
 Lindblad, B. 1956, Stockholms Obs. Ann., 19, No. 7  
 Lo, K.Y., Claussen, M.J. 1983, Nature, 306, 647  
 Mezger, P.G., Duchl, W.J., Zylka, R. 1996, A&A Rev. 7, 289  
 Morris, M., Serabyn, E. 1996, Ann.Rev.A.Ap., 34, 645  
 Oort, J.H. 1965 in Galactic Structure (eds. A Blaauw and M. Schmidt), Chicago: Univ. of Chicago Press, 455  
 Phinney, E.S. 1988, in IAU Symp.136, The Center of the Galaxy (ed. M. Morris), Dordrecht: Kluwer, 543  
 Quinn, P.J., Sussman, G.J. 1985, ApJ, 288, 377  
 Roberts, D.A., Goss, W.M. 1993, ApJ Supp., 86, 113  
 Roberts, D.A., Yusef-Zadeh, F., Goss, W.M. 1996, ApJ, 459, 627  
 Sanders, R.H. 1981, Nature, 294, 427  
 Sanders, R.H. 1992, Nature, 359, 131  
 Syer, D., Clarke, C.J. 1992, MNRAS, 255, 92  
 Schwarz, M.P. 1981, ApJ, 247, 77  
 Schwarz, U.J., Bregman, J.D., van Gorkom, J.H. 1989, A&A, 215, 33  
 Serabyn, E., Lacy 1985, ApJ, 293, 445  
 Serabyn, E., Lacy, J.H., Townes, C.H., Bharat, R. 1988, ApJ, 326, 171  
 Stark, A.A., Gerhard, O.E., Binney, J., Bally, J. 1991, MNRAS, 248, 14p  
 Whitehurst, R. 1988, MNRAS, 233, 529

**Figure 1.** The circumnuclear disk as seen in HCN emission integrated over radial velocity reproduced from the paper of Güsten et al. (1987). The heavy solid contours are in intervals of 0.12 K averaged over 300 km/s. Also shown (light contours) is the 5 GHz radio continuum map by Lo & Claussen (1983) illustrating the ionized filaments. The principal morphological features are labeled. The arrows on the axes indicate the position of the origin (Sgr A\*).

**Figure 2.** A sticky particle simulation of the tidal disruption of a low angular momentum cloud near the Galactic Centre. The clumpy cloud is initially at a distance of 6.5 pc from the galactic centre and moving tangentially with a velocity of 40% that required for a circular orbit. The different frames (left to right) show the passage of the cloud in the orbital plane. The units of length are parsecs with the origin being at the position of the  $2.5 \times 10^6 M_{\odot}$  point mass. The elapsed time in millions of years is indicated for each frame. The elliptical dispersion ring with an asymmetric central cavity is evident after about half a million years. Over the next  $5 \times 10^5$  years the overall shape is maintained but the central cavity gradually closes. The CND can be well-represented by the tidal debris as it appears in the seventh frame ( $t=0.85$ ).

**Figure 3.** These three frames show the CND model at time  $t=0.85$  projected onto the plane of the sky. The offset from the point mass is given in seconds of arc assuming that the Galactic Centre is at a distance of 8.5 kpc (north is up, east is to the left). The structure in the seventh frame of Fig. 2 has been rotated clockwise by 130 degrees, inclined with respect to the plane of the sky by 60 degrees, and the line-of-nodes (shown by the solid line) is rotated to a position angle of 35 degrees with respect to the vertical (north). These are typical projection parameters for the CND where the northwestern side is the near side. The scales are identical to that of Fig. 1 and may be compared directly. The frames show: a) A particle plot where the arrows at the position of the particles indicate the sense and magnitude of the velocity projected onto the plane of the sky (proper motion). b) A contour map of the gas surface density. Units of density are arbitrary, but the contour levels are in equal intervals of 12.5 % of the maximum density. c) A contour map of the radial velocity where solid contours are positive radial velocity (away from the observer) and the dashed contours are negative values. The contours are given in intervals of 40 km/s. Note the positive velocity ridge to the west of Sgr A\*.

**Figure 4.** The radial velocity at the inner edge of the projected dispersion ring seen in Fig. 3 as a function of position angle is shown here by the solid line. Also shown by the unconnected points are the observations of HCN velocities at the inner edge of the CND by Güsten et al. (1987).

**Figure 5.** The ionized filaments as seen in the integrated  $\text{Ne}^+$  emission reproduced from Lacy et al. (1991). This illustrates the ionized filaments in greater detail. Again the principal features are labeled and the dots indicate the extended Northern Arm.

**Figure 6.** Contour map of the 12.4  $\mu\text{m}$  continuum emission of hot dust reproduced from Gezari et al. (1996). The extended Northern Arm is the most conspicuous feature appearing as a partial ellipse wrapping around Sgr A\*. The fainter Eastern arm appears as a morphologically distinct feature in this map.

**Figure 7.** A time sequence of the evolution of tidal debris resulting from the passage of a small cloud ( $r=0.4$  pc) passing within 0.1 pc from the centre of the gravitational field described by eq. 3. Initially the cloud centre is 2.4 pc from the point and moving tangentially with a velocity of 20% that required for a circular orbit. The distance with respect to Sgr A\* is in units of parsecs and the time since the beginning of the infall is given in units of one million years. The cloud is stretched into a long filament which collides with itself at high velocity several times before forming an asymmetric, elliptical dispersion ring. The structure precesses in a sense counter to rotation with an angular frequency of 26 km/s/pc and persists for many rotation periods. The final frame ( $t=0.185$ ) is a reasonable representation of the extended Northern Arm.

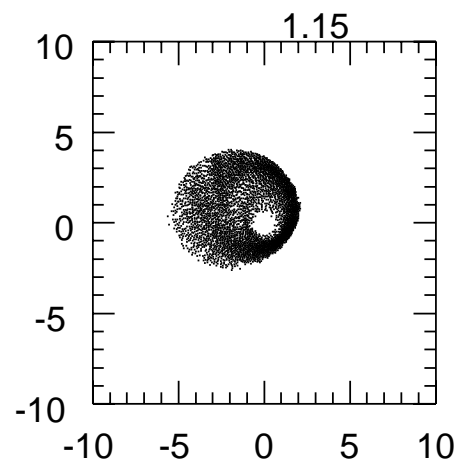
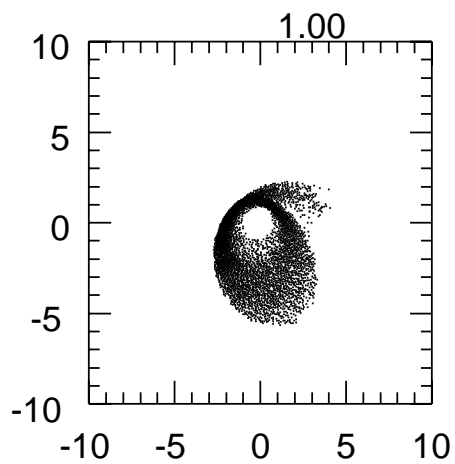
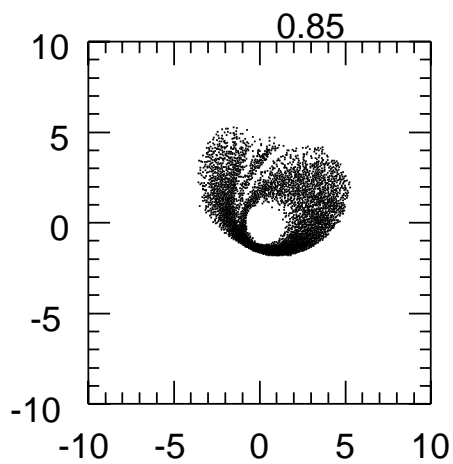
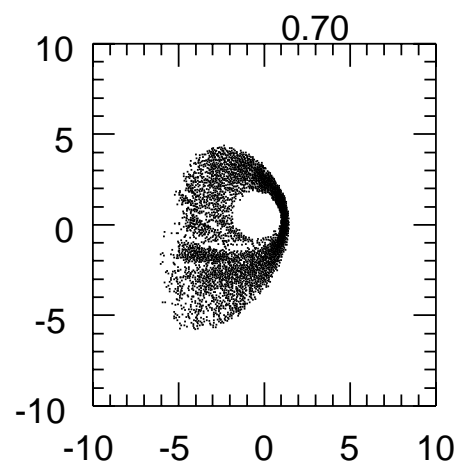
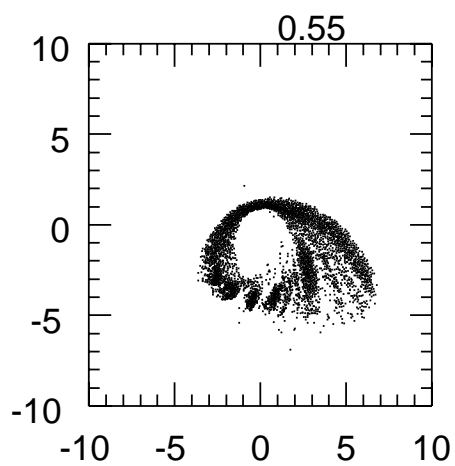
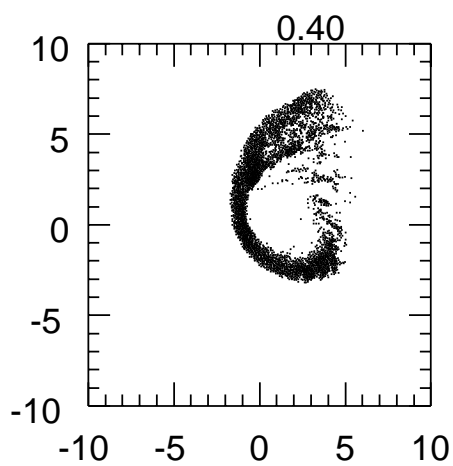
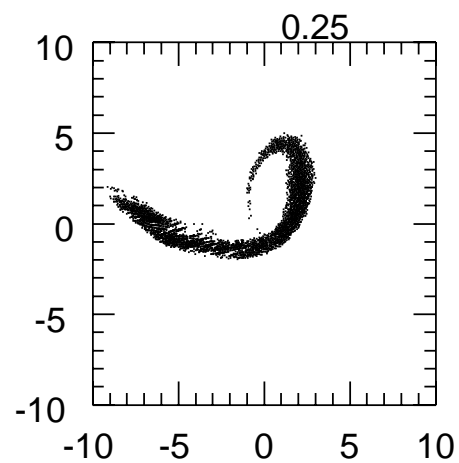
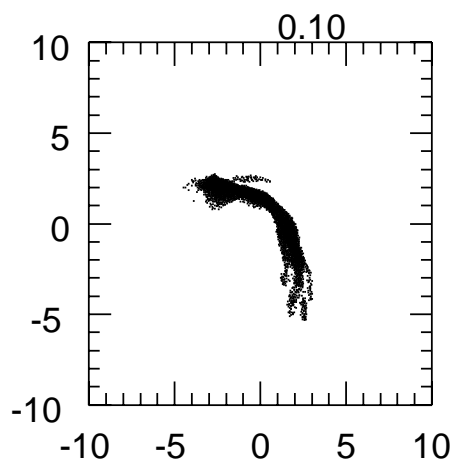
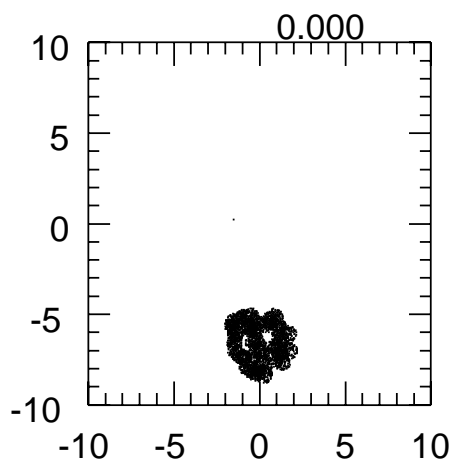
**Figure 8.** Three views of the dispersion ring model of the extended Northern Arm at  $t=0.185$ , the final frame of Fig. 7, projected onto the plane of the sky. The structure as it appears in Fig. 7 is rotated clockwise by 80 degrees, inclined with respect to the sky by 50 degrees, and the line-of-nodes (solid line) is rotated to a position angle of 35 degrees with respect to north. As for the CND model, the northwestern side is the near side. The offsets from the dynamical centre are given in seconds of arc, and the large X marks the position of the point mass. The scales are the same as in Fig. 6 and can be directly compared. As in Fig. 3, the frames show: a) The direction and magnitude of the gas motion projected onto the plane of the sky. b) A contour map of the gas surface density. The units of density are arbitrary but the levels are in equal intervals of 20% of the peak density. The points indicate the positions where the radial velocity has been measured in  $\text{Br}\gamma$  line emission by Herbst et al. (1993). c) A radial velocity contour map. The solid contours are levels of positive velocity in intervals of 40 km/s and dashed contours are of negative velocity also in intervals of 40 km/s.

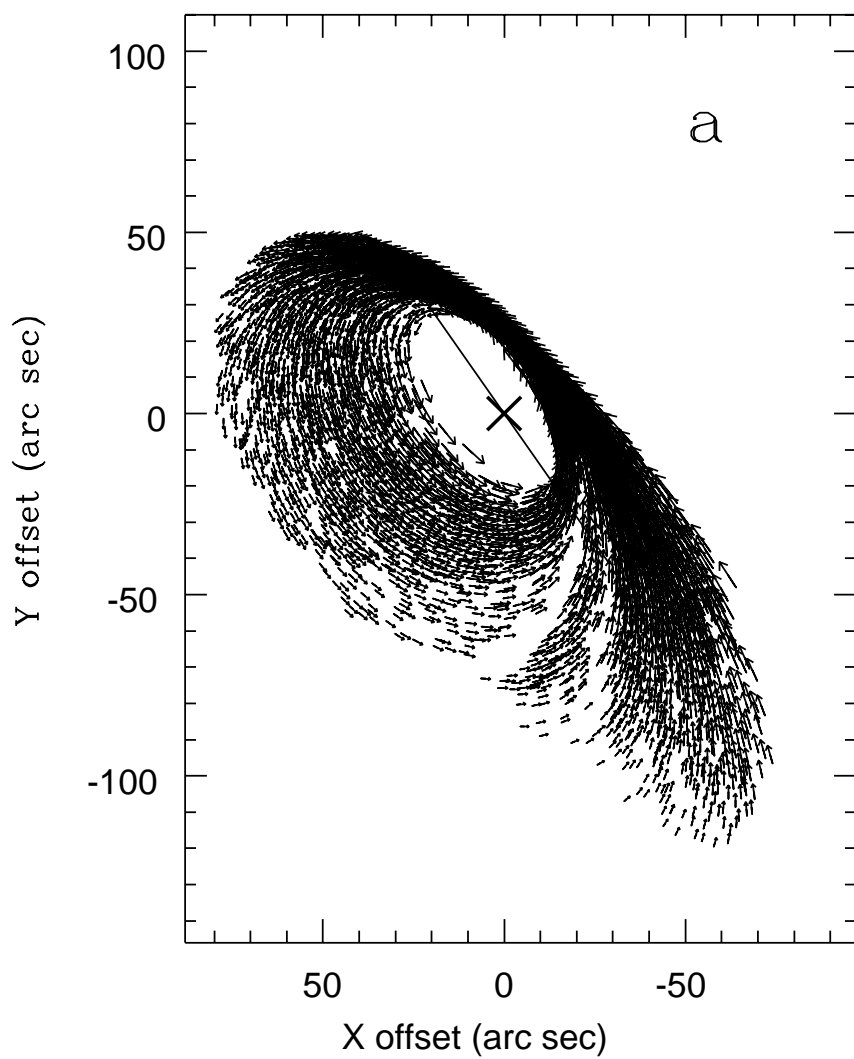
**Figure 9.** The radial velocity of the dispersion ring model for the extended Northern Arm as a function of position angle (with respect to Sgr A\*) is shown by the solid line. Also shown by the unconnected points are the observations of Serabyn & Lacy (1985) and Herbst et al. (1993).

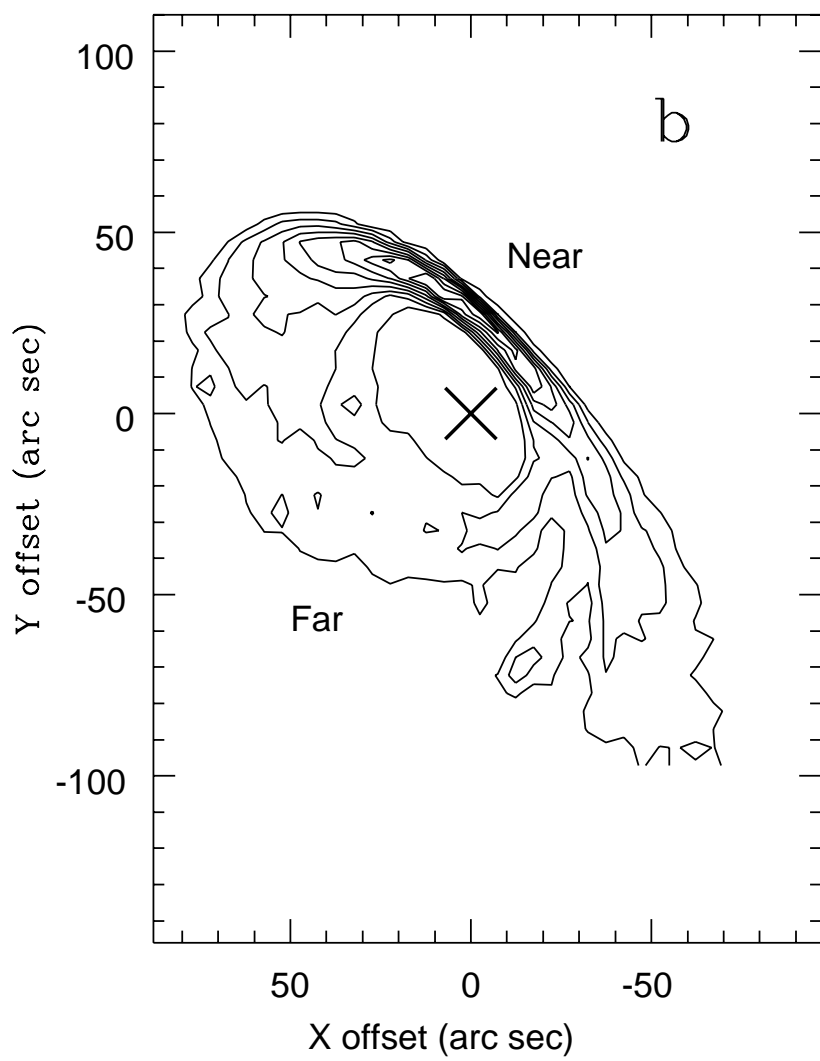
**Figure 10.** The distributions of gas and stars at two different epochs of the Northern Arm simulation. The distance offset from Sgr A\* is given in parsecs. In this simulation stars are allowed to form in regions of strong compression; when a gas particle is converted into a star, the viscous dissipation is turned off and the motion is subsequently determined only by the gravitational force. Frames *a* and *b* show the gas and stars at  $t=0.30$  corresponding to more than one complete precession of the dispersion ring. The gas exhibits the clear structure of the dispersion ring. The stars are phase mixing but are still asymmetrically distributed and reflect the rosette orbit structure. Frames *c* and *d* show the gas and stars at  $t=0.55$ , almost one precessional period later. The gas still exhibits the organized structure of the dispersion ring but the stars are now distributed more symmetrically with respect to the centre.

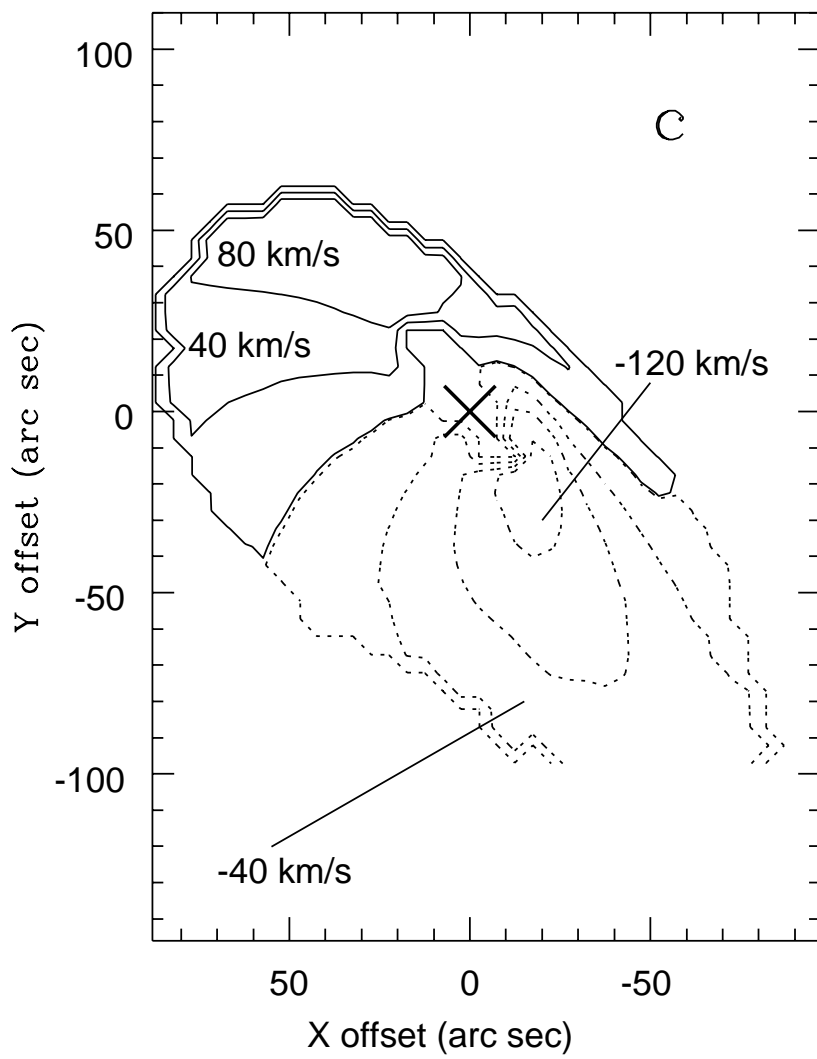
This figure "fg1.gif" is available in "gif" format from:

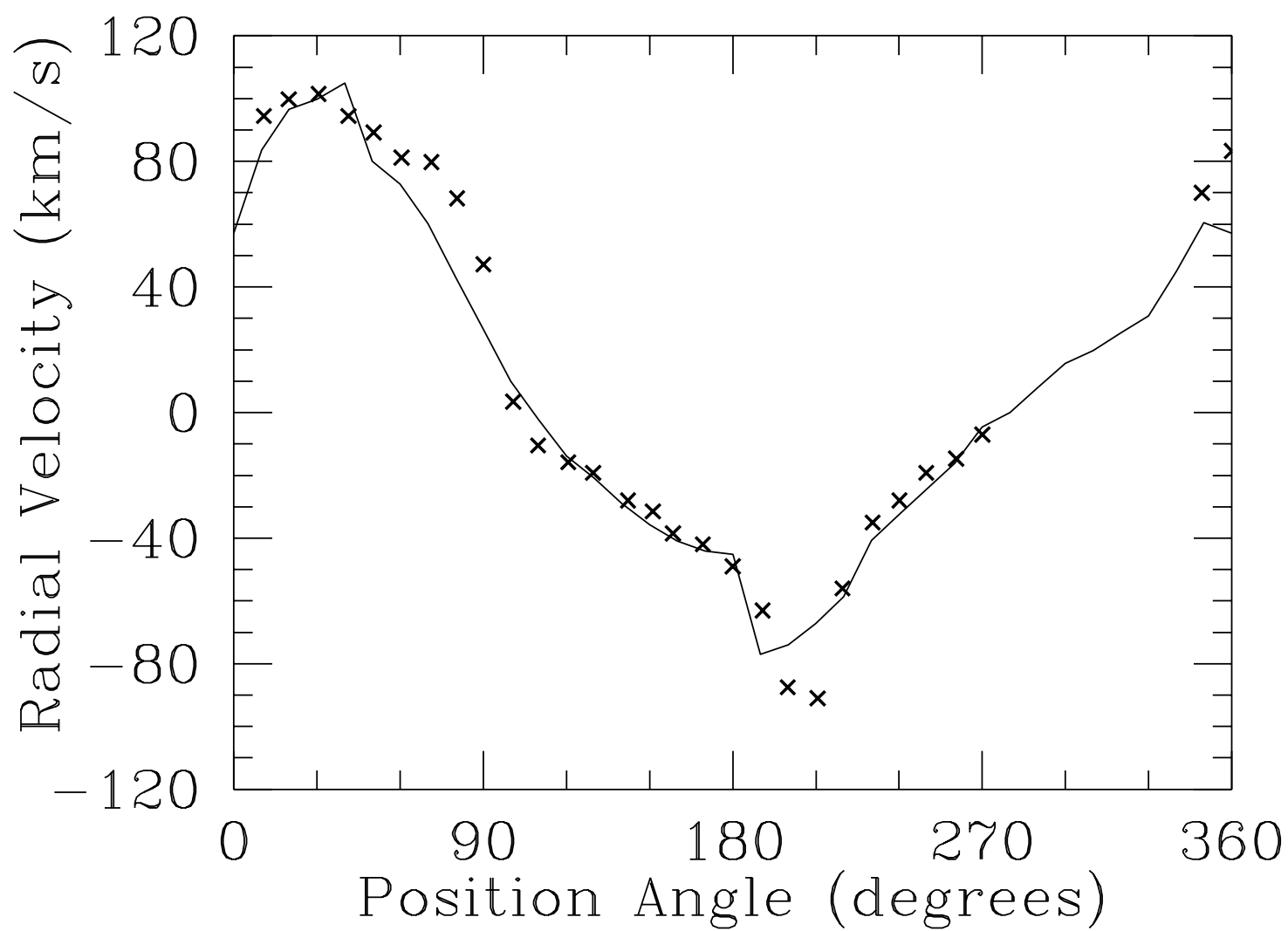
<http://arXiv.org/ps/astro-ph/9708272v1>











This figure "fg5.gif" is available in "gif" format from:

<http://arXiv.org/ps/astro-ph/9708272v1>

This figure "fg6.gif" is available in "gif" format from:

<http://arXiv.org/ps/astro-ph/9708272v1>

